Carbon 104 (2016) 119–124

Contents lists available at ScienceDirect

Carbon

journal homepage: www.elsevier.com/locate/carbon

Surface treatment process applicable to next generation graphene-based electronics

Ki Seok Kim [a], Hyo-Ki Hong [c], Hanearl Jung [d], Il-Kwon Oh [d], Zonghoon Lee [c], Hyungjun Kim [d], Geun Young Yeom [a, b, *], Kyong Nam Kim [e, **]

[a] School of Advanced Materials Science and Engineering, Sungkyunkwan University, 2066 Seobu-ro, Jangan-gu, Suwon-si, Gyeonggi-do 16419, Republic of Korea
[b] SKKU Advanced Institute of Nano Technology (SAINT), Sungkyunkwan University, 2066 Seobu-ro, Jangan-gu, Suwon-si, Gyeonggi-do 16419, Republic of Korea
[c] School of Materials Science and Engineering, Ulsan National Institute of Science and Technology (UNIST), Ulsan 44919, Republic of Korea
[d] School of Electrical and Electronics Engineering, Yonsei University, 50 Yonsei Ro, Seodaemun-gu, Seoul 120-749, Republic of Korea
[e] School of Advanced Materials Science and Engineering, Daejeon University, Yongun-dong, Dong-gu, Daejeon 34520, Republic of Korea

ARTICLE INFO

Article history:
Received 15 January 2016
Received in revised form
20 March 2016
Accepted 25 March 2016
Available online 26 March 2016

ABSTRACT

The polymer residue remaining on chemical-vapor-deposited graphene after its transfer to the substrate and subsequent lithographic patterning tends to cause problems such as decrease in electron mobility, and unwanted doping. In this study, by using a controllable low-energy Ar^+ ion beam (9.5 eV), the residue was cleaned perfectly without damaging the graphene surface. Further, a back-gate graphene field-effect transistor fabricated on the Ar^+-ion-cleaned graphene surface showed about 4 times higher drain current than that showed by a similar transistor fabricated on pristine graphene. We believe that the technique used in this study can be useful in preventing the problems caused by the residue remaining on the graphene surface and can be applied not only to the processing of next-generation graphene-based electronics but also to other 2D materials-based electronic material processing.

© 2016 The Authors. Published by Elsevier Ltd. This is an open access article under the CC BY-NC-ND license (http://creativecommons.org/licenses/by-nc-nd/4.0/).

1. Introduction

Graphene is a two-dimensional conductive nanomaterial consisting of carbon atoms arranged in a honeycomb structure and has an extremely high electron mobility in addition to excellent mechanical strength and high thermal conductivity [1–3]. Owing to the high electron mobility of graphene, graphene-based logic devices are known to show remarkable electrical properties beyond those of complementary metal oxide semiconductor (CMOS) nanoelectronics [4–7].

Currently, for large-area graphene electronics, graphene grown on Cu foils by chemical vapor deposition needs to be transferred to the substrate. For graphene transfer to the substrate, a polymer layer such as that of poly(methyl methacrylate) (PMMA) [8], poly(dimethylsiloxane) (PDMS) [9], poly(bisphenol A carbonate) (PC) [10], or polystyrene (PS) [11] is spin-coated on the graphene surface. Among the various polymers available, PMMA is the most commonly used material for the graphene transfer process [8,12,13]. Further, to fabricate graphene-based electronics, lithographic patterning on the graphene surface is required, and PMMA is also used for such patterning [14–17]. To remove the PMMA layer after graphene transfer to the substrate and lithographic patterning, a solvent such as acetone is used. However, a very thin polymer residue remains on the graphene surface after the polymer layer removal and this residue can cause many problems. For example, the PMMA residue on the graphene surface increases contact resistance, decreases field-effect electron mobility [18], and deteriorates intrinsic properties by doping [19,20]. To remove the PMMA residue from pristine graphene, many techniques such as annealing [16,18,21,22], electrostatic force cleaning [23], and plasma treatment [17,24] have been investigated. However, for PMMA residue removal by annealing, an annealing temperature higher than 350 °C is required in addition to a long annealing time. For electrostatic force cleaning and plasma cleaning, the graphene surface is easily damaged because of the difficulty in controlling the

* Corresponding author. School of Advanced Materials Science and Engineering, Sungkyunkwan University, 2066 Seobu-ro, Jangan-gu, Suwon-si, Gyeonggi-do 16419, Republic of Korea
** Corresponding author.
E-mail addresses: gyyeom@skku.edu (G.Y. Yeom), knam1004@skku.edu (K.N. Kim).

http://dx.doi.org/10.1016/j.carbon.2016.03.054
0008-6223/© 2016 The Authors. Published by Elsevier Ltd. This is an open access article under the CC BY-NC-ND license (http://creativecommons.org/licenses/by-nc-nd/4.0/).

energy of incident particles.

Here, we report a new method for removing the polymer residue on a pristine graphene surface after the transfer of the graphene film from a Cu foil to the substrate. We used a monoenergetic Ar^+ ion beam with an energy of less than ~10 eV for removing the residue on the graphene surface, and the residue could be perfectly removed without damaging the graphene surface. By removing the residue perfectly, we were able to fabricate the field-effect transistors (FETs) showed significantly improved electrical properties.

2. Experimental section

2.1. Preparation of graphene by CVD

Graphene was synthesized on a Cu foil (electroplated Cu film; 99.9 (%); purchased from Wacopa) by chemical vapor deposition. The Cu foil was preheated at 1020 °C with Ar (1000 sccm) and H_2 (100 sccm) gases for 30 min to reduce the Cu surface. Then, CH_4 (5 sccm) was flown into the chamber with Ar (1000 sccm) and H_2 (20 sccm) for 20 min at 1020 °C to grow graphene on the Cu foil; thereafter, Ar (1000 sccm) was flown to cool down the reactor to room temperature. After graphene synthesis, the Cu foil was coated with PMMA (Microchem 950C) and immersed in a Cu etchant (a $FeCl_3$ solution) in order to etch away the Cu foil. When the Cu foil was completely removed, the graphene layer on PMMA was rinsed in deionized water to wash away etchant residues. Then, the PMMA-coated graphene layer was transferred onto a 300-nm-thick SiO_2/Si wafer. PMMA on the SiO_2/Si wafer was removed using acetone after graphene was completely adhered onto the wafer.

2.2. Graphene surface cleaning tool and Ar^+ ion beam energy analysis

The PMMA residue was cleaned using a two-grid inductively coupled plasma (ICP) source in an Ar^+ ion beam system equipped with a mass/energy analyzer (Hiden Analytical Inc., EQP-1000) (Fig. S1, Supplementary information). The first grid of the ICP source located close to the ICP source in the Ar^+ ion beam system was floating, while the second grid located close to the chamber was grounded. The energy of Ar^+ ions extracted from the Ar^+ ion gun was measured by the energy analyzer installed in the mass spectrometer. The sampling orifice of the mass/energy analyzer was installed just behind the substrate; therefore, the exact ion energy distribution on the graphene surface could be measured by operating the Ar^+ ion system without installing the substrate. The Ar^+ ICP source was operated with an Ar gas flow rate of 200–240 sccm and with a 13.56 (%) rf power of 70–500 W. The graphene sample was inserted in the substrate holder through a loadlock for PMMA residue removal without breaking the vacuum.

2.3. Characterization

Graphene surface modification was inspected by Raman spectroscopy (WITEC Alpha 300 M^+) carried out at a wavelength of 532 nm (2.33 eV) and a laser power of 2 mW. The chemical composition of the graphene surface was measured by X-ray photoelectron spectroscopy (XPS, MultiLab 2000, Thermo VG, Mg Kα source). To observe the sp^2 bonding of graphene and sp^3 bonding of the PMMA residue bonded to the graphene surface, the take-off angle of the graphene sample was maintained at 45° and the peak energies were calibrated using the C1s peak at 284.5 eV. The graphene surface roughness was measured by atomic force microscopy (AFM, Dimension 3100, Veeco) under the tapping mode at 512 pixels. Atomic images of pristine graphene and Ar^+-ion-cleaned graphene were observed using high-resolution transmission electron microscopy (HR-TEM, Titan G2 Cube Cs-corrected, FEI) at 80 kV. To observe the HR-TEM image of clean monolayer graphene which was not contaminated by PMMA, monolayer graphene on Cu was directly transferred to TEM grid. (it was possible only for TEM observation) The graphene on Cu was directly transferred to Quantifoil holey carbon TEM grids (SPI supplies, 300 meshes, 2 μm hole size) and was dipped in a solution of sodium persulphate ($Na_2S_2O_8$, a concentration of 0.2 g in 1 ml of water) to etch the underlying copper foil and was then rinsed with deionized water for several times. The current–voltage characteristics of the back-gate graphene FETs were measured using a Keithley 306 electrometer in a probe station.

3. Results and discussion

As shown in Fig. 1a, the Ar^+ ion energy decreased with increasing rf power supplied to the Ar^+ ion source at a fixed Ar gas flow rate of 200 sccm and also decreased with the Ar gas flow rate at an rf power of 500 W (Fig. 1b). The increase of rf power also decreased the ion energy distribution. The decrease in ion energy with increasing rf power is believed to be due to the change in the plasma mode from a capacitively coupled plasma mode to an inductively coupled plasma mode. Further, the decrease in ion energy with increasing gas flow rate is attributed to the increase in plasma density with increasing gas flow rate. By varying the rf power and flow rates for the Ar^+ ion source, the energy of the Ar^+ ion beam could be exactly controlled to be at low values, i.e., from

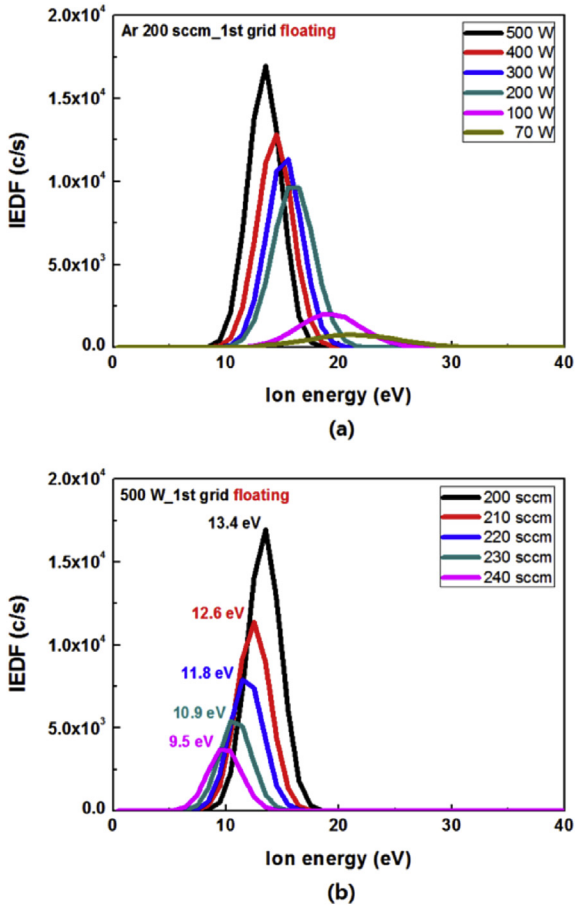

Fig. 1. Ar^+ ion energy distribution of Ar^+ ion source for (a) different rf powers at 200 sccm of Ar gas flow rate and (b) different flow rates at 500 W of rf power measured by ion energy analyzer. (A colour version of this figure can be viewed online.)

9.5 to 13.4 eV and a very low Ar^+ ion energy of 9.5 eV could be obtained with 500 W of rf power and 240 sccm of Ar gas flow rate.

Using the Ar^+ ion beam with different energies, PMMA removal from the graphene surface as well as damage to the surface due to the Ar^+ ion bombardment were investigated. Fig. 2 shows the Raman spectroscopic data for the graphene surface after various Ar^+ ion beam treatments. The data showed a G peak at 1576 cm^{-1} ascribed to graphite and a 2D peak at 2664 cm^{-1} ascribed to sp^2 graphene bonding. In addition, a D peak at 1335 cm^{-1} can be observed and is attributed to defects in graphene (Fig. S2, Supplementary information).

Fig. 2a shows the peak intensity ratio (I_D/I_G) values for ion-beam-treated graphene measured as a function of Ar^+ ion energy and ion beam exposure time. As shown in the Fig., with increasing Ar^+ ion exposure time, I_D/I_G—which depends on the damage to the graphene surface—increased owing to the increased damage to the graphene surface. However, decreasing Ar^+ ion energy decreased I_D/I_G; for an Ar ion energy of 9.5 eV, no change in I_D/I_G was observed, indicating no increase in the damage to the graphene surface until an exposure time of 300 s Fig. 2b shows the Raman spectroscopic data for graphene exposed at 9.5 eV up to 300 s. As shown in the Fig., no change in Raman data was observed, indicating no additional damage to the graphene surface by Ar^+ ion exposure at 9.5 eV. However, as shown in Fig. 2c and d, upon exposure to the 9.5 eV Ar^+ ion beam for 300 s, the positions of G and 2D peaks blue-shifted to higher frequencies by about ~12 cm^{-1} and ~22 cm^{-1}, respectively, whereas the D peak position at ~1335 cm^{-1} did not change. The blue shift of Raman G/2D peaks is generally observed when a p-type doping material on the graphene surface is removed [25]. Therefore, the peak shifts indicated by Raman spectroscopic data in Fig. 2 and caused by Ar^+ ion cleaning can be attributed to the removal of the PMMA residue on the graphene surface. The blue shifts of G and 2D peaks became nearly saturated after cleaning for 180–300 s, possibly indicating the nearly complete removal of the PMMA residue.

Using XPS the degree of PMMA residue removal was investigated by observing the bonding status of carbon atoms in graphene during the Ar^+ ion cleaning. The take-off angle of the XPS spectrometer was set at 45° to determine the PMMA residue status on the graphene surface more accurately. Fig. 3a–d shows XPS C1s narrow-scan data for graphene corresponding to different Ar^+ ion cleaning times from 0 s (pristine) to 300 s after transfer to the substrate (pristine).

As a reference, Fig. 3e shows the XPS C1s narrow-scan data for fresh graphene grown on Cu. As shown in Fig. 3a–d, owing to deconvolution of the C1s peak on the graphene surface, in addition to sp^2 C–C binding energy at 284.5 eV due to graphene, sp^3 C–C binding energies at 285.9–286, 286.9, and 288.8–289 eV mostly due to the PMMA residue were observed; these results are similar to those reported in other researches on the PMMA residue on the graphene surface [26,27]. When the Ar^+ ion cleaning time was 300 s, even though the C1s peak shape was not exactly identical to that observed in Fig. 3e, they were similar owing to the sufficient removal of the PMMA residue on the graphene surface. The percentages of deconvoluted sp^2 and sp^3 C–C bonding measured as a function of the Ar^+ ion cleaning time are shown in Fig. 3f. As shown in Fig. 3f, an increase in the Ar^+ ion cleaning time increased the sp^2 C–C bonding percentage from 63.2 (%) to 86.1 (%) while decreasing

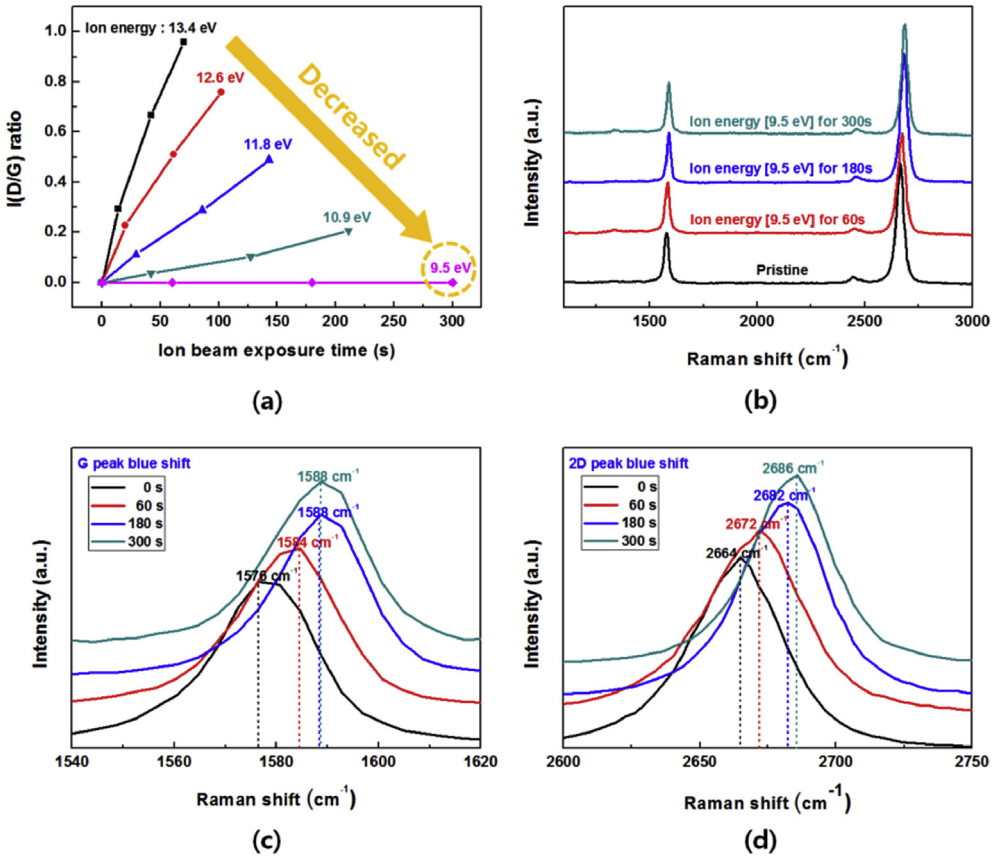

Fig. 2. Raman spectroscopic data for graphene surface after various Ar^+ ion beam treatments. (a) Peak intensity ratio, I_D/I_G, for ion-beam-treated graphene measured as a function of Ar^+ ion energy and ion beam exposure time, (b) Raman spectroscopic data for graphene exposed at 9.5 eV for 0 (pristine), 60, 180, and 300 s, (c) enlarged G peak of Raman spectra, and (d) enlarged 2D peak of Raman spectra. (A colour version of this figure can be viewed online.)

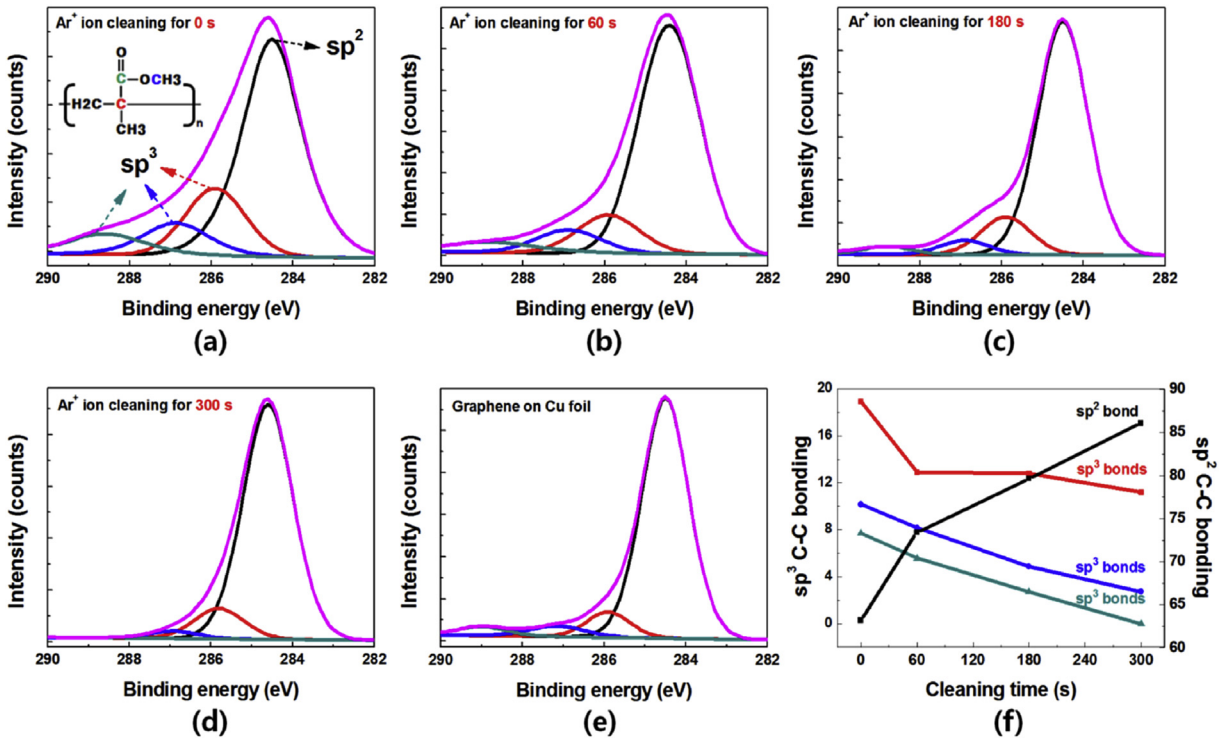

Fig. 3. XPS C1s narrow-scan data for graphene after Ar^+ cleaning for (a) 0 s (pristine), (b) 60 s, (c) 180 s, and (d) 300 s. Panel (e) shows XPS C1s narrow-scan data for fresh graphene on Cu before transfer. XPS C1s data were deconvoluted to sp^2 C–C bonding located at 284.5 eV and sp^3 C–C bonding related to PMMA residue with chemical shifts of $^+$1.4–1.5 (red), $^+$2.4 (blue), and $^+$4.3–4.4 eV (green). Panel (f) shows percentages of sp^2 and sp^3 C–C bonding measured as a function of Ar^+ ion cleaning time. (A colour version of this figure can be viewed online.)

the sp^3 C–C bonding percentage, indicating a decrease in the PMMA residue with increasing Ar^+ ion cleaning time. Exact percentages of the sp^2 and sp^3 C–C bonding are listed in Table S1 (Supplementary information).

The decrease in surface roughness measured by AFM also supported the removal in the PMMA residue upon Ar^+ ion cleaning (Fig. 4).

The AFM root mean square (RMS) surface roughness of graphene transferred to the silicon substrate was measured as 1.21 nm owing to the PMMA residue on the graphene surface. However, after 9.5 eV Ar^+ ion cleaning for 300 s, the AFM surface roughness decreased to 0.34 nm owing to the PMMA residue removal.

The graphene surface before and after Ar^+ ion cleaning was observed using high-resolution transmission electron microscopy (HR-TEM), and the results are shown in Fig. 5a for pristine graphene, (b) for 60 s cleaning, and (c) for 180 s cleaning. As a comparison, the HR-TEM atomic image of a monolayer graphene directly transferred from Cu to TEM grid, therefore, graphene with no PMMA on the surface was taken and the result is shown in Fig. 5 (d) (for the direct transfer from Cu to TEM grid, no PMMA was required). On the corner of each Fig., the fast Fourier transform (FFT) for the graphene monolayer is shown.

As shown by the patterns, for pristine graphene (Fig. 5a), a hazy atomic image was obtained owing to the PMMA residue on the graphene surface after the transfer of graphene from Cu to the substrate. Moreover, as shown by the FFT, cloudy and ring-type patterns indicating an amorphous carbon structure due to the PMMA residue on the graphene surface were observed. Further, as shown by Fig. 5b, after cleaning using the Ar^+ ion beam for 60 s, the haze area decreased and the pattern became sharper showing a dot

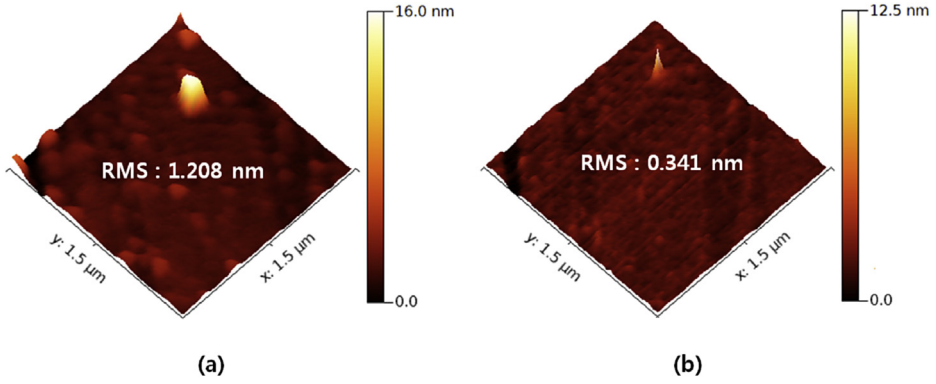

Fig. 4. AFM topographic images of transferred graphene surface observed before and after Ar^+ ion cleaning at 9.5 eV for 300 s. (A colour version of this figure can be viewed online.)

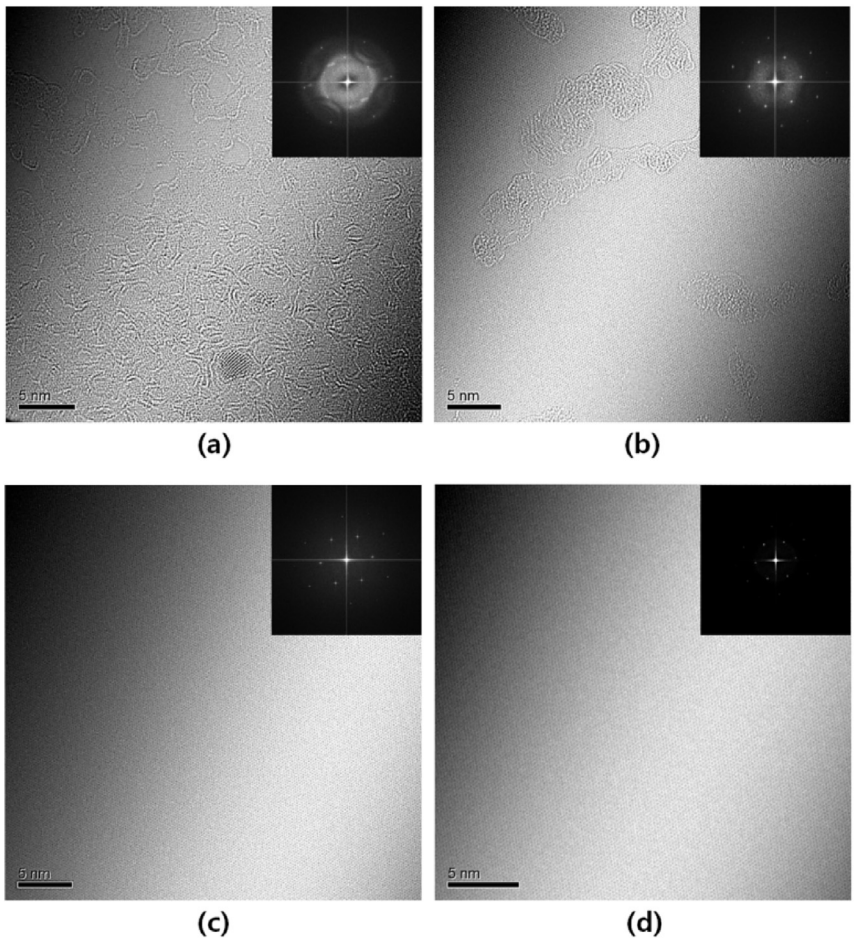

Fig. 5. HR-TEM atomic images of monolayer graphene (a) before Ar^+ ion cleaning (pristine) and after Ar^+ ion cleaning for (b) 60 s and (c) 180 s (d) is the HR-TEM atomic image of a monolayer graphene directly transferred from Cu to TEM grid (therefore, graphene with no PMMA on the surface). On corner of each Fig., fast Fourier transform (FFT) observed for graphene is shown.

pattern with a cloudy amorphous ring pattern due to the removal of a certain amount of the PMMA residue from the graphene surface. Fig. 5c shows a very clean graphene atomic image after the Ar^+ ion cleaning for 180 s. The FFT on the right corner shows only a sharp dot pattern indicating the complete removal of the PMMA residue from the graphene surface. A similar very clean graphene atomic HR-TEM image and a sharp dot pattern of the FFT are also shown for the graphene transferred to TEM grid without PMMA in Fig. 5d, therefore, for the cleanest monolayer graphene. Therefore, compared with other techniques for PMMA residue removal from the graphene surface [16–18,21–24], the use of monoenergetic Ar^+ ions with an energy of 9.5 eV—higher than the PMMA bonding energy on the graphene surface but lower than the sp^2 C–C bonding energy (<22–23 eV) [28–30]—results in more accurate and more complete PMMA residue removal without any damage to graphene bonding.

Fig. 6 shows the drain currents in back-gate graphene FETs fabricated using pristine graphene (black) and graphene cleaned using the Ar^+ ion beam (red) measured as a function of gate voltage. The drain current in the FET after the annealing of pristine graphene (at 450 °C for 2 h to remove the PMMA residue from the pristine graphene surface) is also shown (blue). The fabrication sequences for back-gate graphene FETs are shown in (Fig. S3, Supplementary information).

Fig. 6, the drain current in the back-gate graphene FET fabricated using pristine graphene was lowest, owing to the PMMA residue on

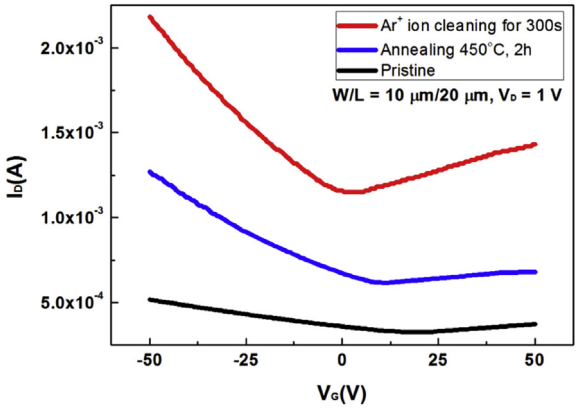

Fig. 6. Drain currents in FETs fabricated using pristine graphene (black) and graphene cleaned using Ar^+ ion beam (red) measured as a function of gate voltage. Drain current in FET fabricated using annealed pristine graphene (pristine graphene was annealed at 450 °C for 2 h to remove PMMA residue) is also shown (blue). Drain current in FETs fabricated using Ar^+-ion-cleaned graphene was about four times that in FETs fabricated using pristine graphene. (A colour version of this figure can be viewed online.)

the graphene contact surface at the source and drain areas. The drain current in the graphene FET increased upon annealing of pristine graphene, possibly owing to the partial removal of the PMMA residue from the graphene contact surface. However, the

drain current in the FET fabricated using annealed graphene was lower than that in the FET fabricated using Ar^+-ion-cleaned graphene, possibly indicating that annealing could not provide sufficient cleaning of graphene contacts compared to the Ar^+ ion cleaning. In addition, the increase of drain current of the back-gate graphene FET in the sequence of pristine graphene, annealed graphene, and Ar^+ ion cleaned graphene is partially related to the removal of scattering effect on the graphene surface because the electron mobility which can be seen by the change of the slope between V_G-I_D was also improved by the removal of PMMA residue. In addition, as the PMMA residue is removed, the charge neutrality point (Dirac point) has shifted from 19 V for pristine graphene, to 11 V after the annealing at 450 °C for 2 h, and further to near 0 V after the Ar^+-ion-cleaning. Previous researches on PMMA residue removal also showed the shift of Dirac point to near 0 V as the PMMA residue is removed on the graphene surface [17,23].

4. Conclusions

Graphene layers are generally transferred from a Cu foil by using PMMA, and the transferred graphene surface contains PMMA residue that cannot be easily removed by wet cleaning techniques. In this study, by using a controllable low-energy Ar^+ ion beam (9.5 eV), the PMMA residue on the graphene surface was almost perfectly removed without damaging the graphene surface. The results were confirmed by Raman spectroscopy, AFM, XPS, and TEM. The graphene FETs showed a high drain current owing to the lower contact resistance of cleaned graphene. We believe that the Ar^+ ion cleaning technique presented herein can be very useful in low temperature, high throughput, large area and Si compatible process for fabricating various graphene-based electronic devices.

Acknowledgments

This research was supported by the Ministry of Trade, Industry and Energy (MOTIE; 10049065) and Korea Semiconductor Research Consortium (KSRC) support program for the development of future semiconductor devices. This work was also supported by the Industry technology R&D program of MOTIE/KEIT. [10050501, Development of laser assisted hybrid inorganic deposition system for flexible organic device passivation] and Basic Science Research Program through the National Research Foundation of Korea funded by the Ministry of Education (2015R1D1A4A01020731).

Appendix A. Supplementary data

Supplementary data related to this article can be found at http://dx.doi.org/10.1016/j.carbon.2016.03.054.

References

[1] K.S. Novoselov, A.K. Geim, S.V. Morozov, D. Jiang, Y. Zhang, S.V. Dubonos, et al., Electric field effect in atomically thin carbon films, Science 306 (5696) (2004) 666–669.
[2] K. Novoselov, A.K. Geim, S. Morozov, D. Jiang, M.K.I. Grigorieva, S. Dubonos, et al., Two-dimensional gas of massless Dirac fermions in graphene, Nature 438 (7065) (2005) 197–200.
[3] Y. Zhang, Y. Tan, H.L. Stormer, P. Kim, Experimental observation of the quantum Hall effect and Berry's phase in graphene, Nature 438 (7065) (2005) 201–204.
[4] V.V. Cheianov, V. Fal'ko, B.L. Altshuler, The focusing of electron flow and a Veselago lens in graphene p-n junctions, Science 315 (5816) (2007) 1252–1255.
[5] S.K. Banerjee, L.F. Register, E. Tutuc, D. Basu, S. Kim, D. Reddy, et al., Graphene for CMOS and beyond CMOS, Appl. Proc. IEEE 98 (12) (2010) 2032–2046.
[6] S.K. Banerjee, L.F. Register, E. Tutuc, D. Reddy, A.H. MacDonald, Bilayer pseudospin field-effect transistor (BiSFET): a proposed new logic device, IEEE Electron Device Lett. 30 (2) (2009) 158–160.
[7] S. Tanachutiwat, J. Ung Lee, W. Wang, C.Y. Sung, Reconfigurable multi-function logic based on graphene pn junctions, Des. Autom. Conf. (DAC) (2010) 883–888.
[8] X. Li, W. Cai, J. An, S. Kim, J. Nah, D. Yang, et al., Large-area synthesis of high-quality and uniform graphene films on copper foils, Science 324 (5932) (2009) 1312–1314.
[9] K.S. Kim, Y. Zhao, H. Jang, S.Y. Lee, J.M. Kim, K.S. Kim, et al., Large-scale pattern growth of graphene films for stretchable transparent electrodes, Nature 457 (7230) (2009) 706–710.
[10] Y. Lin, C. Jin, J. Lee, S. Jen, K. Suenaga, P. Chiu, Clean transfer of graphene for isolation and suspension, ACS Nano 5 (3) (2011) 2362–2368.
[11] E.H. Lock, M. Baraket, M. Laskoski, S.P. Mulvaney, W.K. Lee, P.E. Sheehan, et al., High-quality uniform dry transfer of graphene to polymers, Nano Lett. 12 (1) (2011) 102–107.
[12] X. Li, Y. Zhu, W. Cai, M. Borysiak, B. Han, D. Chen, et al., Transfer of large-area graphene films for high-performance transparent conductive electrodes, Nano Lett. 9 (12) (2009) 4359–4363.
[13] Z. Yan, J. Lin, Z. Peng, Z. Sun, Y. Zhu, L. Li, et al., Toward the synthesis of wafer-scale single-crystal graphene on copper foils, ACS Nano 6 (10) (2012) 9110–9117.
[14] M. Ishigami, J. Chen, W. Cullen, M. Fuhrer, E. Williams, Atomic structure of graphene on SiO2, Nano Lett. 7 (6) (2007) 1643–1648.
[15] L.A. Ponomarenko, F. Schedin, M.I. Katsnelson, R. Yang, E.W. Hill, K.S. Novoselov, et al., Chaotic Dirac billiard in graphene quantum dots, Science 320 (5874) (2008) 356–358.
[16] Y. Lin, C. Lu, C. Yeh, C. Jin, K. Suenaga, P. Chiu, Graphene annealing: how clean can it be? Nano Lett. 12 (1) (2011) 414–419.
[17] Y. Lim, D. Lee, T. Shen, C. Ra, J. Choi, W.J. Yoo, Si-compatible cleaning process for graphene using low-density inductively coupled plasma, ACS Nano 6 (5) (2012) 4410–4417.
[18] A. Pirkle, J. Chan, A. Venugopal, D. Hinojos, C. Magnuson, S. McDonnell, et al., The effect of chemical residues on the physical and electrical properties of chemical vapor deposited graphene transferred to SiO2, Appl. Phys. Lett. 99 (12) (2011) 122108.
[19] D.B. Farmer, Y. Lin, A. Afzali-Ardakani, P. Avouris, Behavior of a chemically doped graphene junction, Appl. Phys. Lett. 94 (21) (2009) 213106.
[20] J. Chen, M. Ishigami, C. Jang, D.R. Hines, M.S. Fuhrer, E.D. Williams, Printed graphene circuits, Adv. Mater 19 (2007) 3623–3627.
[21] Z. Cheng, Q. Zhou, C. Wang, Q. Li, C. Wang, Y. Fang, Toward intrinsic graphene surfaces: a systematic study on thermal annealing and wet-chemical treatment of SiO2-supported graphene devices, Nano Lett. 11 (2) (2011) 767–771.
[22] C. Gong, H.C. Floresca, D. Hinojos, S. McDonnell, X. Qin, Y. Hao, et al., Rapid selective etching of PMMA residues from transferred graphene by carbon dioxide, J. Phys. Chem. C 117 (44) (2013) 23000–23008.
[23] W.J. Choi, Y.J. Chung, S. Park, C. Yang, Y.K. Lee, K. An, et al., A simple method for cleaning graphene surfaces with an electrostatic force, Adv. Mater 26 (4) (2014) 637–644.
[24] N. Peltekis, S. Kumar, N. McEvoy, K. Lee, A. Weidlich, G.S. Duesberg, The effect of downstream plasma treatments on graphene surfaces, Carbon 50 (2) (2012) 395–403.
[25] H. Shin, W.M. Choi, D. Choi, G.H. Han, S. Yoon, H. Park, et al., Control of electronic structure of graphene by various dopants and their effects on a nanogenerator, J. Am. Chem. Soc. 132 (44) (2010) 15603–15609.
[26] S. Yumitori, Correlation of C1s chemical state intensities with the O1s intensity in the XPS analysis of anodically oxidized glass-like carbon samples, J. Mater. Sci. 35 (1) (2000) 139–146.
[27] C. Ton-That, A. Shard, D. Teare, R. Bradley, XPS and AFM surface studies of solvent-cast PS/PMMA blends, Polymer 42 (3) (2001) 1121–1129.
[28] J. Kotakoski, D. Santos-Cottin, A.V. Krasheninnikov, Stability of graphene edges under electron beam: equilibrium energetics versus dynamic effects, ACS Nano 6 (1) (2011) 671–676.
[29] J. Kotakoski, C. Jin, O. Lehtinen, K. Suenaga, A. Krasheninnikov, Electron knock-on damage in hexagonal boron nitride monolayers, Phys. Rev. B 82 (11) (2010) 113404.
[30] A. Zobelli, A. Gloter, C. Ewels, G. Seifert, C. Colliex, Electron knock-on cross section of carbon and boron nitride nanotubes, Phys. Rev. B 75 (24) (2007) 245402.